AUT Journal of Mechanical Engineering

AUT J. Mech. Eng., 6(4) (2022) 579-596
DOI: 10.22060/ajme.2022.20917.6025

Numerical Evaluation on Blood Rheological Behavior in a Realistic Model of Aneurysmal Coronary Artery

A. Rafiei, M. Saidi*

[1] Department of Mechanical Engineering, Razi University, Kermanshah, Iran

ABSTRACT: The aim of this study is to evaluate the blood rheological behavior within a coronary artery aneurysm in detail. The three-dimensional model was reconstructed from computed tomography angiography images of a 43-year-old man with a coronary artery aneurysm on the bifurcation. First, the effects of blood dynamic viscosity on the hemodynamic characteristics in the aneurysmal coronary artery were studied. Then, a comparison between Newtonian and non-Newtonian viscosity models was carried out using four non-Newtonian blood models, namely the Carreau, Modified Casson, Cross, and Carreau-Yasuda models. The results have been presented in the form of velocity contours, streamlines, pressure drop variation, wall shear stress, and oscillatory shear index. The outcomes showed that a 20% change in the Newtonian blood viscosity leads to almost up to 12% alters in the aneurysm wall shear stress and nearly 15-18% changes in the value of the other sections. The decrement of the blood viscosity declines the aneurysm rupture risk by reducing blood pressure and wall shear stress. Additionally, among studied viscosity models, the Modified Casson model predicts the highest value of average wall shear stress in all parts except for the aneurysm, whereas, the highest value in the aneurysm is related to the Carreau model, close to 5.3% greater than the Modified Casson. Moreover, the average wall shear stress in the Newtonian state is the lowest in comparison with non-Newtonian models.

Review History:

Received: Dec. 23, 2021
Revised: Oct. 14, 2022
Accepted: Oct. 16, 2022
Available Online: Oct. 23, 2022

Keywords:

Coronary artery aneurysm
Computational fluid dynamics
Non-Newtonian fluid
Blood viscosity
Wall shear stress

1- Introduction

Heart diseases and especially Coronary Artery Diseases (CAD), such as atherosclerosis and Coronary Artery Aneurysms (CAA), are the leading cause of death in developed countries [1]. The CAA -a local dilation of the coronary artery- is defined when the coronary artery diameter becomes greater than 1.5 times its locally normal diameter [2]. Children's Kawasaki disease and atherosclerosis are the leading cause of CAAs, while sometimes CAA has a congenital origin [3, 4]. Risks of aneurysm presence include myocardial infarction due to distal embolization and stenosed downstream segments of the arteries. On the other hand, the prolonged presence of blood in the aneurysm can disturb blood flow which in more severe cases leads to myocardial ischemia [4, 5]. Studying the rheological behavior of the blood and determination of flow dynamics changes by using Computational Fluid Dynamics (CFD), plays an important role in better understanding, diagnosis, and even treatment of many cardiovascular diseases [6-8]. Therefore, many researchers have conducted numerical studies on arterial hemodynamics. In a numerical and three-dimensional (3D) study by Johnston et al. [9] on blood rheology in the four different right coronary arteries, with the aim of achieving a better approximation of Wall Shear Stress (WSS) in the areas with low shear rates, the use of non-Newtonian viscosity models was recommended. Lorenzini [10] studied a steady laminar blood flow through a vessel numerically by employing the Casson and Power-law models and compared the results with the Newtonian model. He concluded that considering blood as a Newtonian fluid at high shear rates is partly acceptable. However, for the study of blood flow within the coronary arteries or cerebral arteries, non-Newtonian viscosity models, especially the Casson model, provide higher accuracy. Blood flow in a carotid artery usually covers a wide range of shear rates, so a constant viscosity model may not be able to express the blood behavior in the different shear rates [11]. Therefore, Fan et al. [11] numerically investigated 3D and pulsatile non-Newtonian blood flow in a carotid artery. They used the Newtonian, non-Newtonian Casson, and a hybrid model. Their results showed that at the beginning of the cycle, the WSS distribution was similar for all three models, and regions with low shear stress were formed almost similarly. Wang and Li [12] investigated the effect of increased viscosity on hemodynamics in a non-realistic aortic aneurysm. They indicated that increasing the Newtonian blood viscosity (from 0.0027 Pa.s to 0.0097 Pa.s) increases the peak value of WSS significantly during the systole phase. In a numerical study implemented by Skiadopoulos et al. [13], three various viscosity models, including Newtonian,

*Corresponding author's email: msaidi@razi.ac.ir

Quemada, and Casson were utilized for evaluating blood viscous behavior in an Iliac bifurcation. They applied a time-dependent velocity profile for the inlet and a predefined flow rate boundary condition for bifurcation outlets. The result of their study revealed that the WSS distribution pursues a pattern regardless of the chosen viscosity models, whereas there is a direct relation between WSS magnitude and blood rheological models, as well as shear rate. According to their results, the average WSS values calculated by the Casson and Quemeda models were 9.81% and 7.98% higher than the values of the Newtonian model at peak systole. Caballero and Lain [14] simulated a steady laminar flow of Newtonian and non-Newtonian blood in a patient-specific thoracic aorta. Their study showed that the lowest WSS occurred near the aortic arch and distal areas of the branches for all models. Apostolidis et al. [15] compared the Casson model with the Newtonian model in a coronary artery. Their study showed considerable differences (up to 50%) between the WSS of Newtonian and non-Newtonian viscosity models. To investigate the effects of shear-thinning fluid properties on hemodynamic characteristics, Oliveira et al. [16] simulated the unsteady flow of Newtonian and non-Newtonian blood in an abdominal aortic aneurysm at rest. They found that the shear-thinning behavior affects the velocity distribution and the WSS. Razavi et al. [17] aimed to study blood rheology by simulating unsteady laminar blood flow in a 3D model of the middle cerebral artery of a 75-year-old male. They compared the Newtonian model with the Carreau-Yasuda model for blood and concluded that the Newtonian and non-Newtonian models have no notable differences; therefore, the Newtonian model for blood in the middle cerebral artery is acceptable. Bahrami and Norouzi [18] conducted a numerical 3D study on hemodynamics in a left coronary bifurcation. In their study, a physiological realistic pulsatile coronary pressure was considered as an inlet boundary condition. Furthermore, they employed the Casson model for the blood, and hyperelastic as well as rigid models for the vessel wall. Kopernik and Tokarczyk [19] studied a laminar steady two-phase flow of non-Newtonian blood in a 3D model of a vessel with 60% stenosis. They adopted the Power-law and the Herschel-Bulkly models for non-Newtonian Blood and concluded that the two-phase Herschel–Bulkley model is appropriate for describing the blood flow within medium-sized stenosed vessels.

Although hemodynamics and rheological studies have been at the center of researchers' attention recently, it seems that the blood rheological behavior in coronary artery aneurysms rarely has been studied in the literature. In addition, since aneurysms are commonly asymmetric and have complex shapes, using the idealized model of aneurysms leads to underestimating the realistic features of the aneurysm's geometry.

In the present study, the influence of blood rheology on the flow field and hemodynamic characteristics in a realistic model of a human Left Coronary Artery (LCA) with a fusiform aneurysm on the bifurcation have been investigated by changing the dynamic viscosity and comparing different viscosity models. The results of the first part of the present study can aid clinical decision-making in the evaluation of coronary artery aneurysms. Moreover, the comparative study on rheological models can play a constructive role in future similar studies by providing a capture of using various viscosity models to assess the hemodynamics in aneurysmal coronary arteries.

2- Materials and Methods

2- 1- Reconstruction of the CAA model

In order to better capture the geometric features in the arteries, a patient-specific 3D model of a human left coronary artery with an aneurysm was reconstructed from a patient's data in Bistoon Hospital, Kermanshah, Iran. The process of geometry reconstruction has been shown in Fig. 1. The images by Digital Imaging and Communications in Medicine standard format (DICOM) used for this 3D reconstruction were acquired from Computed Tomography Angiography (CT Angiography) of a 43-years-old man with an aneurysm covering the bifurcation on the LCA (Fig. 1(a)). As can be seen in Fig. 1(b), the 3D reconstruction and segmentation were conducted utilizing the geometrical reconstruction software: Materialise mimics 19.0 (Materialise NV, Leuven, Belgium). Then, for more modifications, such as surface smoothening and removing the small sub-branches without sufficient resolution, the model was exported to the Materialise 3-Matic 11.0 software (Materialise NV, Leuven, Belgium). Next, to define the different zones, the realistic coronary artery model was exported with the Initial Graphics Exchange Specification format (IGES) format. The fully reconstructed model after smoothing and segmentation which was applied for simulations is observable in Fig. 1(c).

2- 2- Meshing process

To introduce the zones and produce a proper mesh, the 3D reconstructed model by IGES format was imported to ICEM CFD 17.1 software (ICEM CFD, ANSYS package, ANSYS Inc). The coronary artery model was divided into Left Main (LM), Aneurysm, Left Circumflex (LCX), Left Anterior Descending (LAD), and a sub-branch of LAD called Diagonal. After zone introduction, an unstructured tetrahedral mesh was adopted for the 3D model of the coronary artery in three steps. In the first step, a proper surface mesh was produced by the Octree method. Then, the Delaunay method was employed to enhance the volume mesh quality. Finally, for better accuracy of results near the vessel walls, five layers of boundary layer mesh with a 1.2 aspect ratio were created. The structure of generated mesh with 1,484,494 elements is presented in Fig. 2. To ensure that the results are mesh independent, a grid independency test has been performed through steady and non-Newtonian blood flow using the Carreau viscosity model. For this purpose, six different computational grids, namely Case 1 to Case 6, respectively, with various counts of cells (course to fine), were employed and their detailed properties are summarily provided in Table 1. As can be easily seen in Fig. 3, which shows the

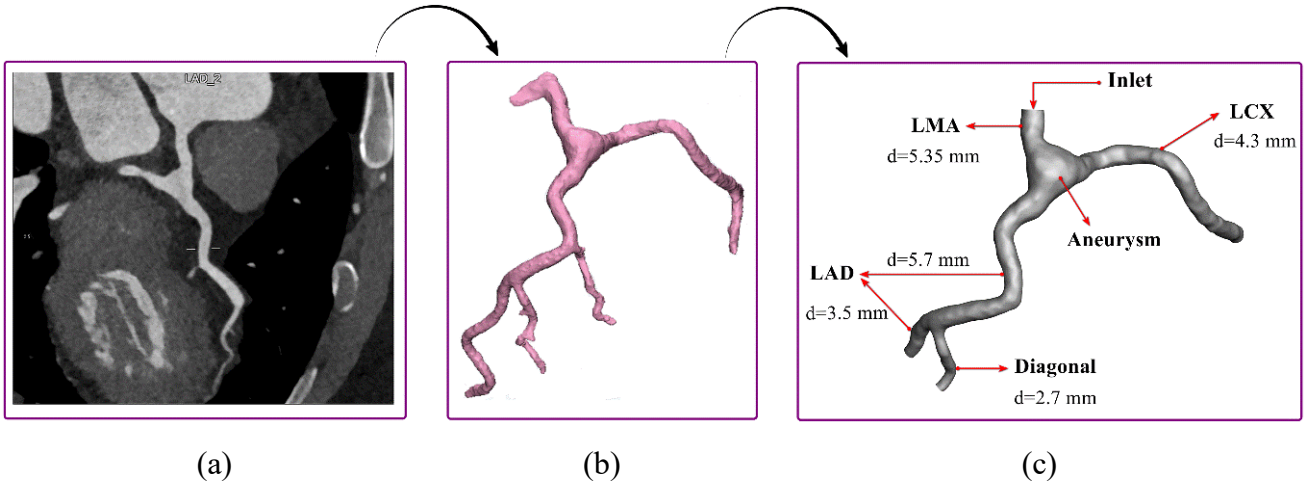

Fig. 1. a) 2D CT angiography image and b) Developed 3D model in 3-Matic software c) Parts of 3D repaired and reconstructed model of the left coronary artery with aneurysm

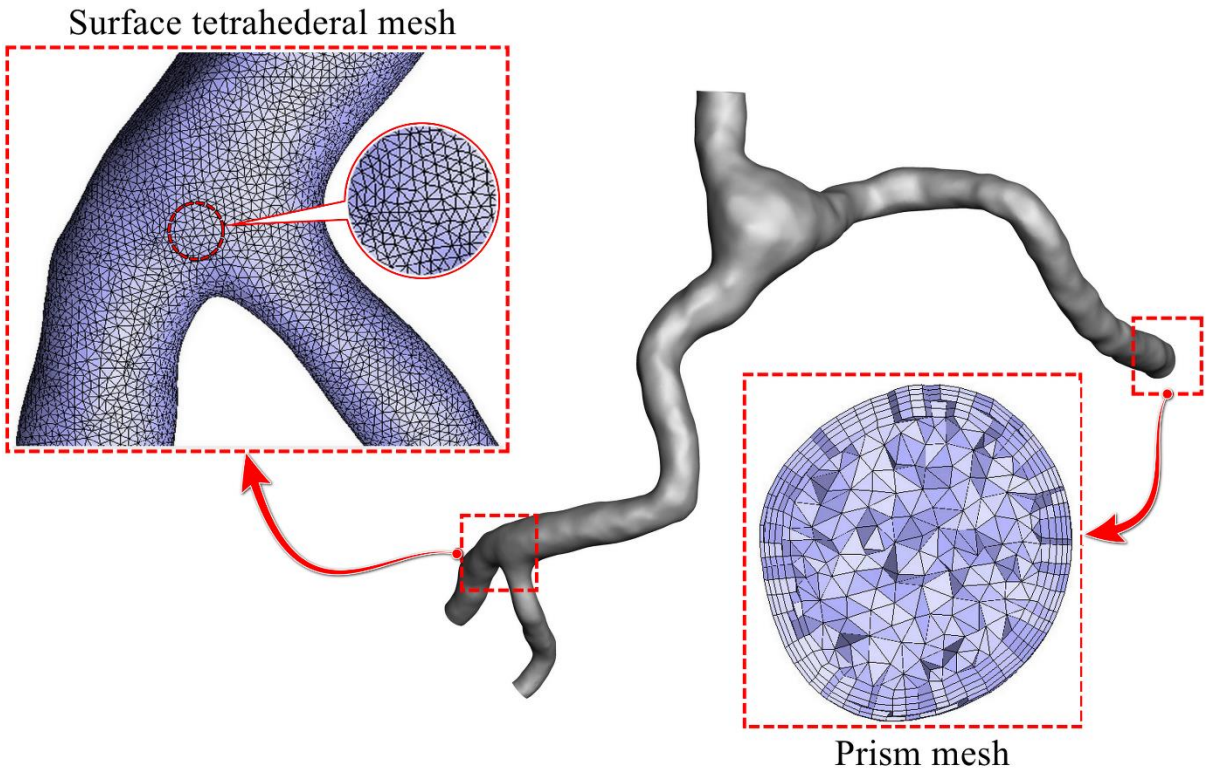

Fig. 2. Generated grid for the computational domain

Table 1. Details of the applied meshes for the grid independency test

Grids	Count of cells	Max size of cells [mm]	Prism layers info		
			Δy^* [mm]	Aspect ratio	Count of layers
Case 1	229,297	0.6	0.09	1.2	5
Case 2	568,416	0.41	0.07	1.2	5
Case 3	1,484,494	0.265	0.05	1.2	5
Case 4	2,575,919	0.227	0.04	1.2	5
Case 5	3,614,240	0.2	0.035	1.2	5
Case 6	5,686,380	0.17	0.026	1.2	5

* Height of the first cell of the prism mesh near the vessel wall

average WSS on the whole of the aneurysmal LCA, there is no significant discrepancy between the results acquired by Case 3 and finer meshes. Thus, Case 3 with 1,484,494 cells was chosen for the rest of the simulations. Meanwhile, it is evident from Fig. 3 that using high cell numbers for meshing the geometry did not cause an unusual jump in the results, so there is no concern about corruption and degrading the numerical solution.

2- 3- Governing equations and numerical solution approach

The unsteady and laminar flow of Newtonian and non-Newtonian blood is modeled by solving momentum and continuity equations. By disregarding the gravitational and volumetric forces acting on the fluid, the governing equations for incompressible flow are written as follows:

$$\rho\left(\frac{\partial \mathbf{V}}{\partial t}+\left(\mathbf{V}.\nabla\right)\mathbf{V}\right)=-\nabla P-\nabla.\tau \tag{1}$$

$$\nabla\cdot\mathbf{V}=0 \tag{2}$$

In the above equations, ρ and V are the density and velocity vectors, respectively. Also, t is the time, P is the pressure, and τ is the shear stress. With the help of the current form of momentum equation, different non-Newtonian viscosity models can be included. Conspicuously, the blood dynamic viscosity, $\mu=\mu\left(\dot{\gamma}\right)$, depending on the shear rate. For non-Newtonian models, it alters based on their viscosity equations which are presented in the following. Whereas, if blood is considered as a Newtonian fluid, its viscosity will tend to be a constant value which is equal to μ_∞ = 0.00345 Pa.s [8, 20]. Moreover, the blood density was assumed to be constant and set to $\rho=1060\,\mathrm{kg/m^3}$ [21-23]. Additionally, ANSYS FLUENT 17.1 (ANSYS FLUENT, ANSYS package, ANSYS Inc) [24] was employed to solve the governing equations based on the finite volume method, using a computer with 32 GB RAM and 12 parallel threads of Core i7-4960X CPU. Also, Pressure-Velocity equations coupling was performed by the Semi-Implicit Method for Pressure Linked Equations (SIMPLE) scheme, and the second-order and upwind second-order discretization schemes were used for pressure and momentum interpolation, respectively. Finally, these discretized equations were solved by the second-order implicit method. Simulations were conducted for three cardiac cycles with a time step equal to $\Delta T = 0.002$ s, but to avoid initial effects, only the results of the third cycle have been considered. Convergence criteria were set equal to 10^{-6} in a maximum of ten iterations per each time step. As mentioned formerly, in the first step, to study the effects of various blood viscosity on the aneurysm hemodynamic behaviors, blood viscosity was assumed to be 0.00276 Pa.s, 0.00345 Pa.s, and 0.00414 Pa.s (20% increase and decrease in the viscosity). Furthermore, by assuming the blood as a non-Newtonian fluid, four non-Newtonian viscosity models (Carreau, Modified Casson, Cross, and Carreau-Yasuda models) were

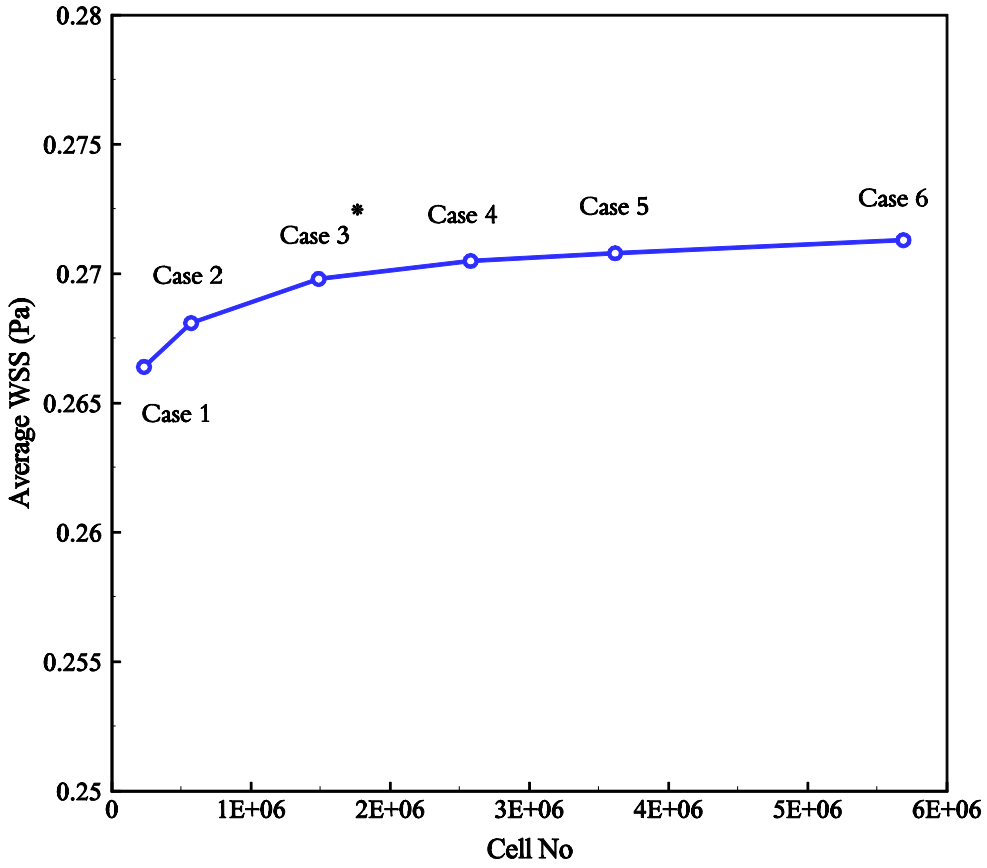

Fig. 3. Mesh study utilizing Average WSS of the LCA model

compared with each other and with the Newtonian model as a comparative study. Blood viscosity models and their details, including the input parameters of each model, are given in Table 2. In addition, Fig. 4 illustrates the relation between blood viscosity and shear rate for all employed models. The red solid line denotes the Newtonian model which is independent of the shear rate.

2- 4- Oscillatory shear index

The wall shear stress has different effects on vascular endothelial cells over time [18]. In fact, WSS is one of the most important characteristics of fluid dynamics that is mainly used in the hemodynamic analysis of the blood flow in the arteries but is not able to accurately describe some phenomena like plaque formation or progression of atherosclerosis [28]. Hence, Ku et al. [29] introduced the Oscillatory Shear Index (OSI) for the oscillating nature of the blood in the arteries. This dimensionless numerical parameter is defined for the WSS in pulsatile flows. The OSI indicates regions where the vector of WSS deviates from its dominant axial direction during the cardiac cycle [18, 29, 30]. The OSI is defined as [30]:

$$OSI = 0.5 \times \left(1 - \frac{\left| \int_0^T \vec{\tau}_w \, dt \right|}{\int_0^T \left| \vec{\tau}_w \right| dt} \right) \tag{3}$$

Where T and $\vec{\tau}_w$ denote the period of the cardiac cycle and the WSS vector, respectively. Depending on the deviation of the WSS vector, OSI varies from 0 to 0.5, in which the value of 0 denotes regions without flow oscillation, and the value of 0.5 is for completely oscillating zones [30]. In general, the regions with OSI of more than 0.1 are among the high-risk areas prone to thrombosis risk and atherosclerotic plaque formation [31].

2- 5- Boundary conditions

To study the flow in the CAA at various times of a cardiac cycle, a time-varying uniform velocity profile was applied as an inlet boundary condition, which is obtained by dividing the real volumetric blood flow rate of the LCA [32] by the inlet cross-section. The inlet velocity profile of the LCA has been represented in Fig 5. In addition, zero static constant

Table 2. Blood viscosity models with details

Model	Effective viscosity, μ	Input parameters
Newtonian [9]	$\mu = \mu_\infty$	$\mu_\infty = 0.00345$ Pa.s
Carreau [25]	$\mu(\dot{\gamma}) = \mu_\infty + \frac{\mu_0 - \mu_\infty}{\left[1+(\lambda\dot{\gamma})^2\right]^{\frac{1-n}{2}}}$	$\mu_0 = 0.056$ Pa.s $\mu_\infty = 0.00345$ Pa.s $\lambda = 3.313$ s $n = 0.3568$
Modified Casson [26]	$\mu(\dot{\gamma}) = \sqrt{\mu_C} + \left(\frac{\sqrt{\tau_y}}{\sqrt{\beta}+\sqrt{\dot{\gamma}}}\right)^2$	$\mu_C = 0.004$ Pa.s $\tau_y = 0.021$ Pa $\beta = 11.5\,\mathrm{s}^{-1}$
Cross [27]	$\mu(\dot{\gamma}) = \mu_\infty + \frac{\mu_0 - \mu_\infty}{1+(\lambda\dot{\gamma})^n}$	$\mu_0 = 0.0364$ Pa.s $\mu_\infty = 0.00345$ Pa.s $\lambda = 0.38$ s $n = 1.45$
Carreau-Yasuda [25]	$\mu(\dot{\gamma}) = \mu_\infty + \frac{\mu_0 - \mu_\infty}{\left[1+(\lambda\dot{\gamma})^\alpha\right]^{\frac{1-n}{\alpha}}}$	$\mu_0 = 0.056$ Pa.s $\mu_\infty = 0.00345$ Pa.s $\lambda = 1.902$ s $n = 0.22$ $\alpha = 1.25$

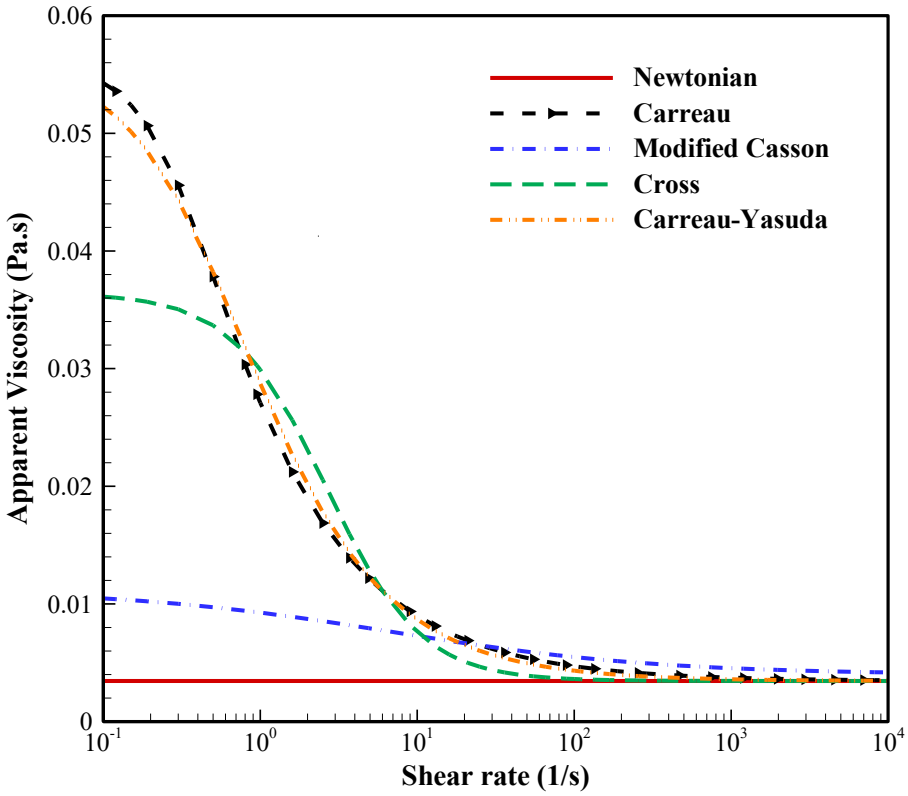

Fig. 4. Viscosity changes versus shear rate for different blood rheological models

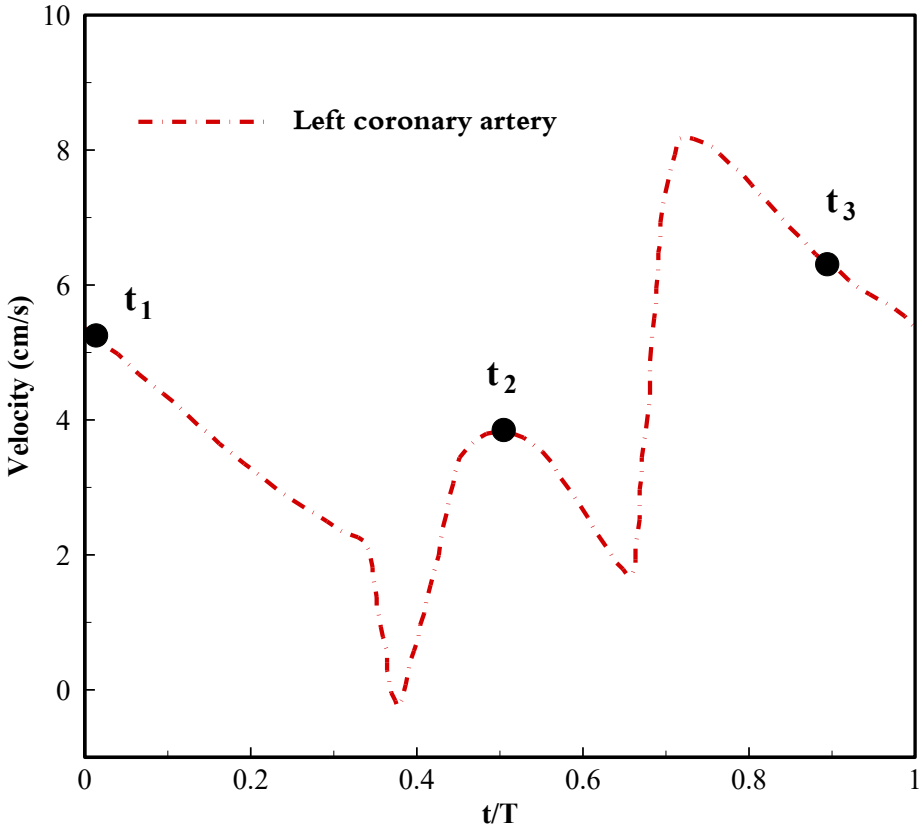

Fig. 5. Cardiac pulsatile velocity applied for the inlet boundary condition

pressure boundary conditions were implemented at the outlets [33]. By selecting the appropriate CFD domain in the simulations, assuming walls to be rigid can provide acceptable hemodynamics in the coronary arteries [34]. Hence, walls were considered to be rigid, and the No-Slip condition was set for them. It is worth mentioning that the maximum Reynolds number (Re) was related to the Newtonian state ($\mu = 0.00276$ Pa.s) within the CAA lesion at $t/T = 0.72$ which was less than 400.

2- 6- Validation of the numerical method

In order to validate our simulations, an experimental and numerical study conducted by Gijsen et al. [35] was used. Therefore, the laminar, fully developed, and steady flow of the Newtonian and non-Newtonian blood in a 2D model of the carotid artery was simulated numerically, and the present results were compared with the experimental results of Gijsen et al. [35]. To fulfill this purpose, in the results verification section, the blood density was assumed to equal 1410 kg/m^3, and blood viscosity in the Newtonian state was set to 0.0029 Pa.s. Also, the Carreau-Yasuda model was adopted to reflect the non-Newtonian behavior of the blood in the carotid artery. Fig. 6 demonstrates an acceptable agreement between the axial velocity profile for both Newtonian and non-Newtonian blood flow within the common carotid obtained numerically and the experimental data.

3- Results and Discussion

In this study, 3D, laminar, and unsteady blood flow through a realistic model of the left coronary artery with an aneurysm located at the bifurcation has been simulated. The effects of blood rheology on aneurysmal hemodynamics in terms of velocity, pressure drop, wall shear stress, and oscillatory shear index have been investigated in detail.

3- 1- Newtonian model

As mentioned previously, in the first part of this work, the blood was assumed as a Newtonian fluid, and by considering three different values of blood viscosity, the influence of viscosity change on the hemodynamic parameters has been studied. Histogram of LCA pressure drop at t_1, t_2 (peak of the systole), and t_3 for mentioned three viscosities are shown in Fig. 7(a). By increasing the blood viscosity, the pressure drop rises along the LCA which is more noticeable at high shear rates. The pressure drop during the cycle is also shown in Fig. 7(b) which can be seen is almost similar to the inlet velocity profile.

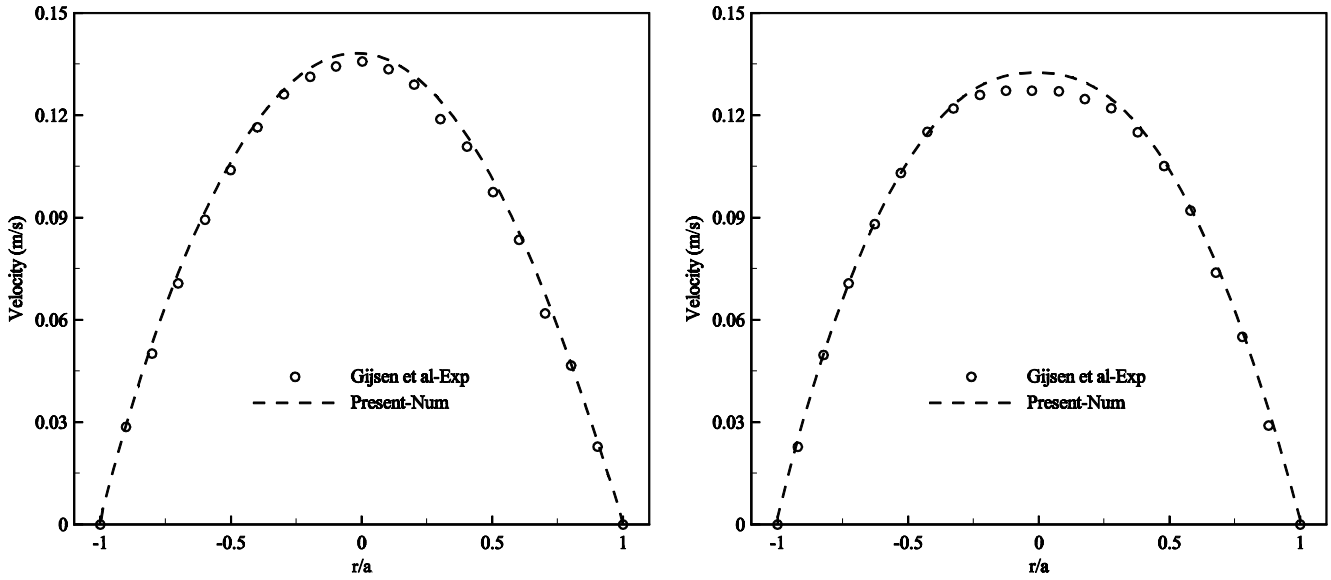

Fig. 6. Comparison between axial velocity profile captured numerically and experimental data

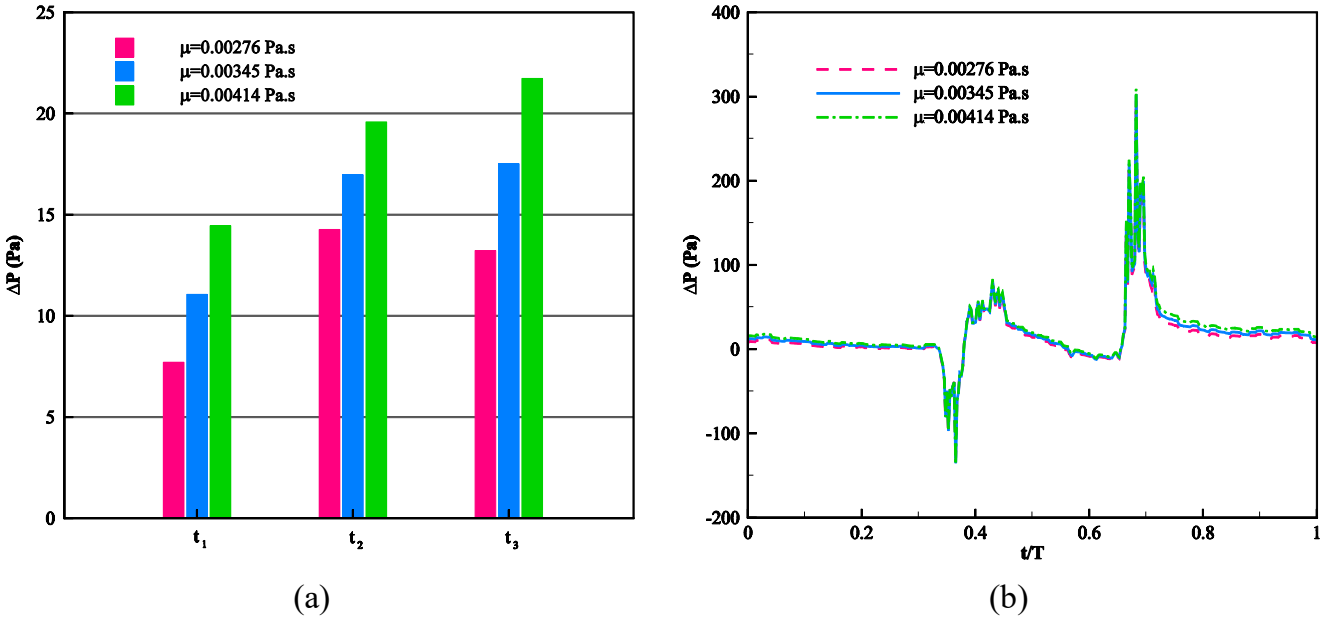

Fig. 7. LCA pressure drop for various viscosities a) at different times and b) during the cardiac cycle

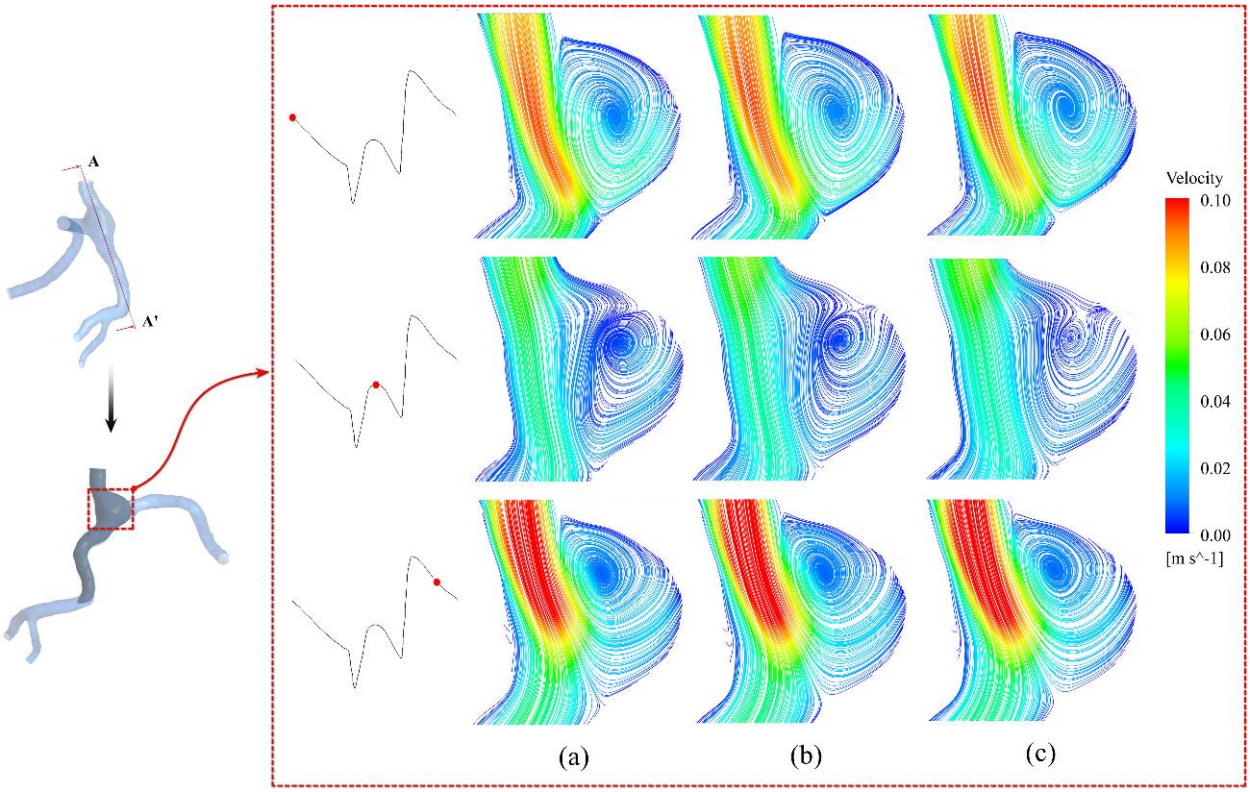

Fig. 8. 2D velocity contour and streamlines of blood flow with the viscosity equal to a) 0.00276 Pa.s, b) 0.00345 Pa.s and c) 0.00414 Pa.s at different pulsatile phases

Table 3. Area average values of WSS over a cardiac cycle in the various segments of LCA for various viscosities of the Newtonian model

Dynamic Viscosity [Pa.s]	Wall shear stress [Pa]			
	Aneurysm	LCX	LAD	Diagonal
μ = 0.00276	0.078	0.189	0.173	0.207
μ = 0.00345	0.085	0.227	0.206	0.248
μ = 0.00414	0.090	0.265	0.240	0.288

Fig. 8 depicts the 2D velocity contours and streamlines of the Newtonian blood flow in the aneurysm zone (on plate A-A') in different viscosities at t_1, t_2, and t_3. Clearly, increasing the dynamic viscosity leads to a decrement in the fluid velocity due to the increase in frictional resistance between the fluid layers. Blood flow in most aneurysms is affected by disorders such as reversal and recirculating flow, so this is accepted that the vortex formation phenomenon occurs in most aneurysms. Considering Fig. 8, it is visible that the 20% change in viscosity did not make an impressive change in the vortex structure of the aneurysm as well as its position.

Table 3 provides the area average WSS values over a cardiac cycle in the aneurysm, LCX, LAD, and Diagonal arteries, and Fig. 9 shows the variation of average WSS for the three mentioned viscosities during the cardiac cycle. The 20% change of viscosity leads to alter in the WSS in the aneurysm up to 12% (at decelerating phase or t_3), and a 15-18% change in the WSS in the LCX, LAD, and Diagonal branches, directly. It's worth mentioning, the relation between the change of the blood viscosity and the WSS is nonlinear because by increasing the viscosity, the velocity gradient decreases near the walls.

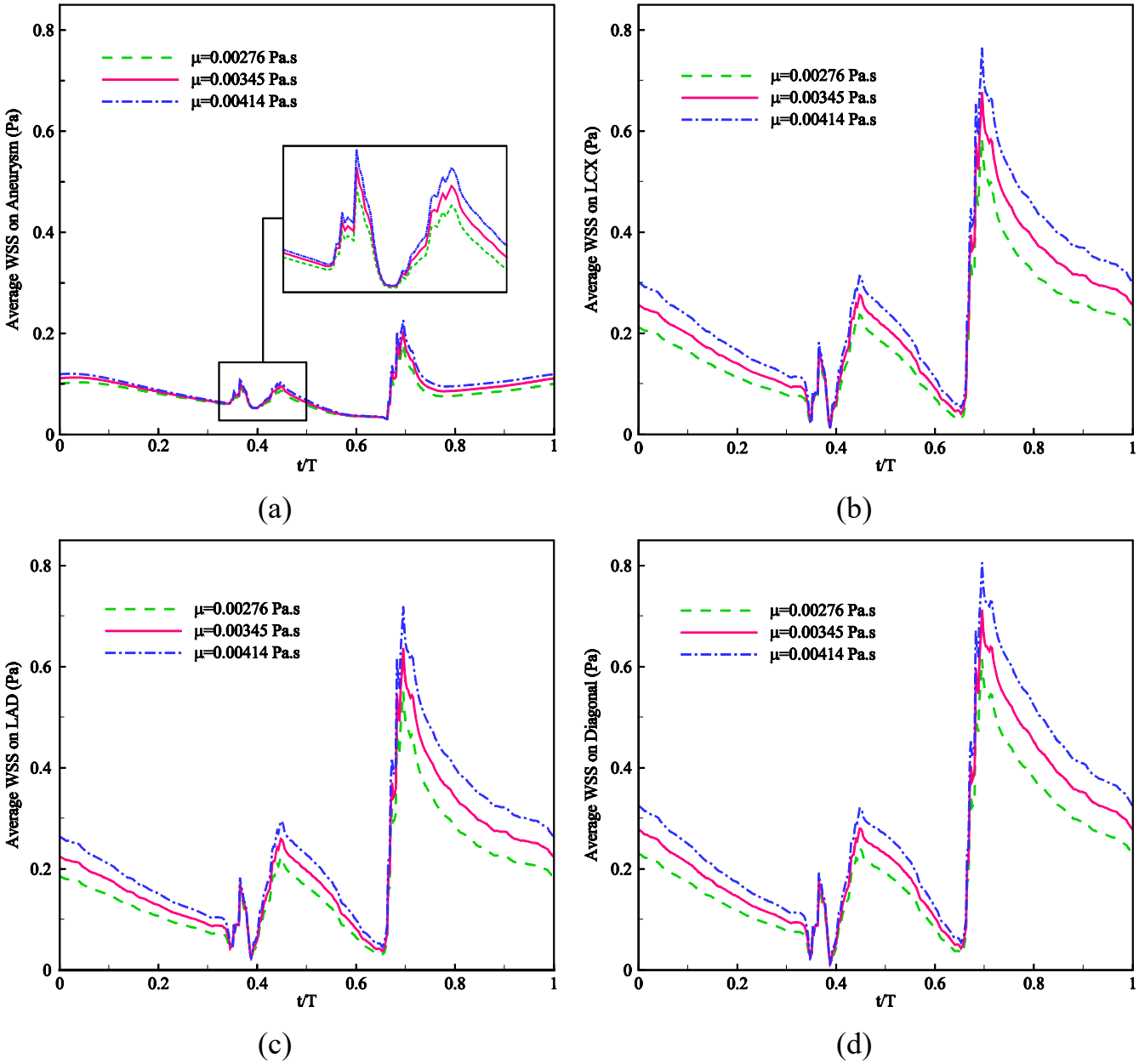

Fig. 9. Variation of average WSS in the a) Aneurysm, b) LCX, c) LAD, and d) Diagonal for different viscosities of the Newtonian blood model during the cardiac cycle

It is clear that the presence of an aneurysm in the bifurcation and its complicated hemodynamic conditions cause discrepancies in the variation of average WSS in the aneurysm than in other zones. According to Fig. 9(a), which belongs to the aneurysm, the WSS diagram exhibits a relatively different behavior than other arteries at t_1 and t_3. In fact, unlike other parts of the LCA, the average WSS of the aneurysm has an upward trend with decreasing velocity in the diastole region, which is due to the change of vortex position in the aneurysm at t_1 compared to t_2.

The contours of WSS for different viscosities at the t_1, t_2, and t_3 have been presented in Fig 10. The decrement and increment of the WSS in the aneurysmal LCA are clearly visible by decreasing and increasing the blood viscosity, respectively.

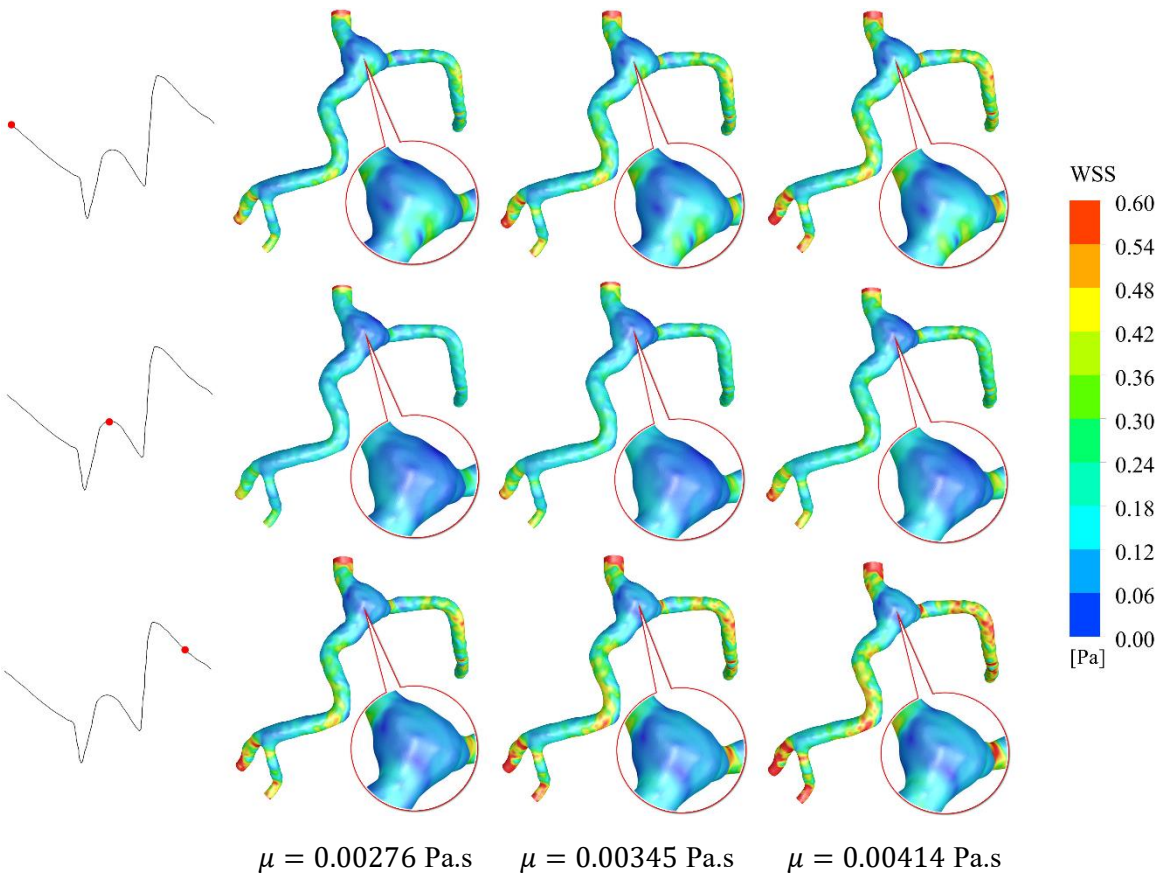

Fig. 10. Contours of WSS distribution for different viscosities of the Newtonian blood model at various pulsatile phases

The blood viscosity influences the WSS, and there is a correlation between the WSS and the risk of aneurysm rupture [12, 36]. Therefore, according to the above-obtained results, in the absence of using invasive and semi-invasive methods for aneurysms treatment, controlling the blood viscosity and WSS with the help of blood-thinning medicines and anticoagulants, has an effect on preventing the growth and rupture of the aneurysms.

3- 2- non-Newtonian model

In the second part of this study, a comparison between non-Newtonian blood models was carried out considering Carreau, Modified Casson, Cross, and Carreau-Yasuda models, and results were compared with the Newtonian model with dynamic viscosity equal to 0.00345 Pa.s. The 2D contours of the blood viscosity for non-Newtonian models and the shear rate for all viscosity models in the aneurysm zone (A-A' plane) have been shown in Fig. 11 and Fig. 12, respectively. By comparing Fig. 11 and Fig. 12 and also considering Fig. 4, it can be observed that among the non-Newtonian viscosity models, the Modified Casson model has the lowest viscosity at shear rates less than 10 s^{-1}. In the areas with strain rates of approximately 0.7 to 6 s^{-1}, the maximum value of the viscosity is correlated to the Cross model. On the other hand, in the regions with strain rain of more than 10 s^{-1}, this model has the minimum viscosity compared to other non-Newtonian viscosity models. It should be noted that the correlation between viscosity and shear rate is almost similar in the Carreau and Carreau-Yasuda models.

Generally, the maximum blood shear rate in the desired LCA is related to the LM and is approximately equal to 1500 s^{-1}, which occurs at the peak of diastole ($t/T = 0.72$). The minimum shear rate also belongs to the aneurysm zone at t/T = 0.385, which is roughly equal to 0.1 s^{-1}. The minimum value of blood strain rate near the vessel wall is lesser than 14 s^{-1}, which corresponds to the aneurysm region at $t/T = 0.385$.

Area average WSS values over the cardiac cycle in the Aneurysm, LCX, LAD, and Diagonal branches for different viscosity models are listed in Table 4. Additionally, the variation of WSS during the cycle for the Newtonian and non-Newtonian viscosity models in all segments is presented separately in Fig. 13. In all parts of the studied LCA, the Newtonian model always estimates the lowest value of the WSS (around 9 to 59% less than non-Newtonian models depending on various segments). As shown in Fig. 13(a), which is focused on the aneurysm zone, not much difference can be seen between the average WSS of the non-Newtonian viscosity models. In such a way that, their graphs overlap at some points over the cardiac cycle. Since the blood shear rate in the aneurysm at these times is about 20 to 25 s^{-1} and the blood viscosity for the non-Newtonian viscosity models are

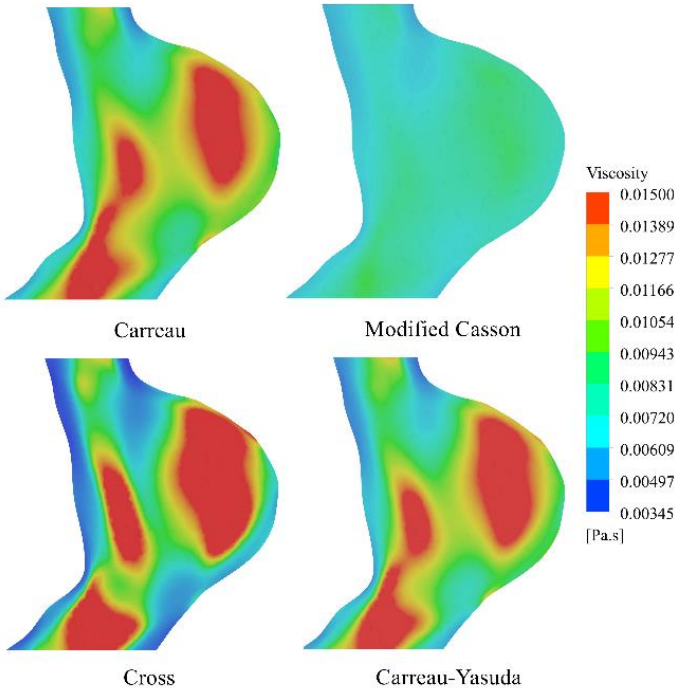

Fig. 11. 2D contours of blood viscosity in the aneurysm for different non-Newtonian viscosity models at t2 (peak of the systole)

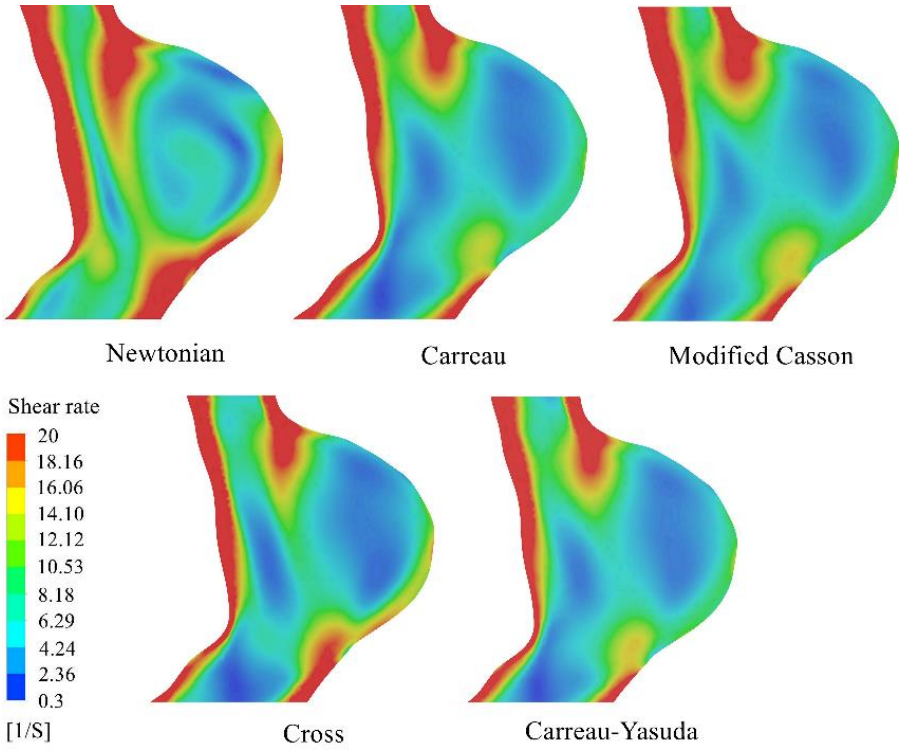

Fig. 12. 2D contours of blood shear rate in the aneurysm for different viscosity models at t2 (peak of the systole)

Table 4. Area average values of WSS over a cardiac cycle in the different segments of LCA for various viscosity models

Viscosity models	Wall shear stress [Pa]			
	Aneurysm	LCX	LAD	Diagonal
Newtonian (μ = 0.00345 Pa.s)	0.084	0.227	0.206	0.248
Carreau	0.113	0.334	0.305	0.341
Modified Casson	0.107	0.360	0.327	0.376
Cross	0.103	0.259	0.236	0.270
Carreau-Yasuda	0.111	0.310	0.284	0.318

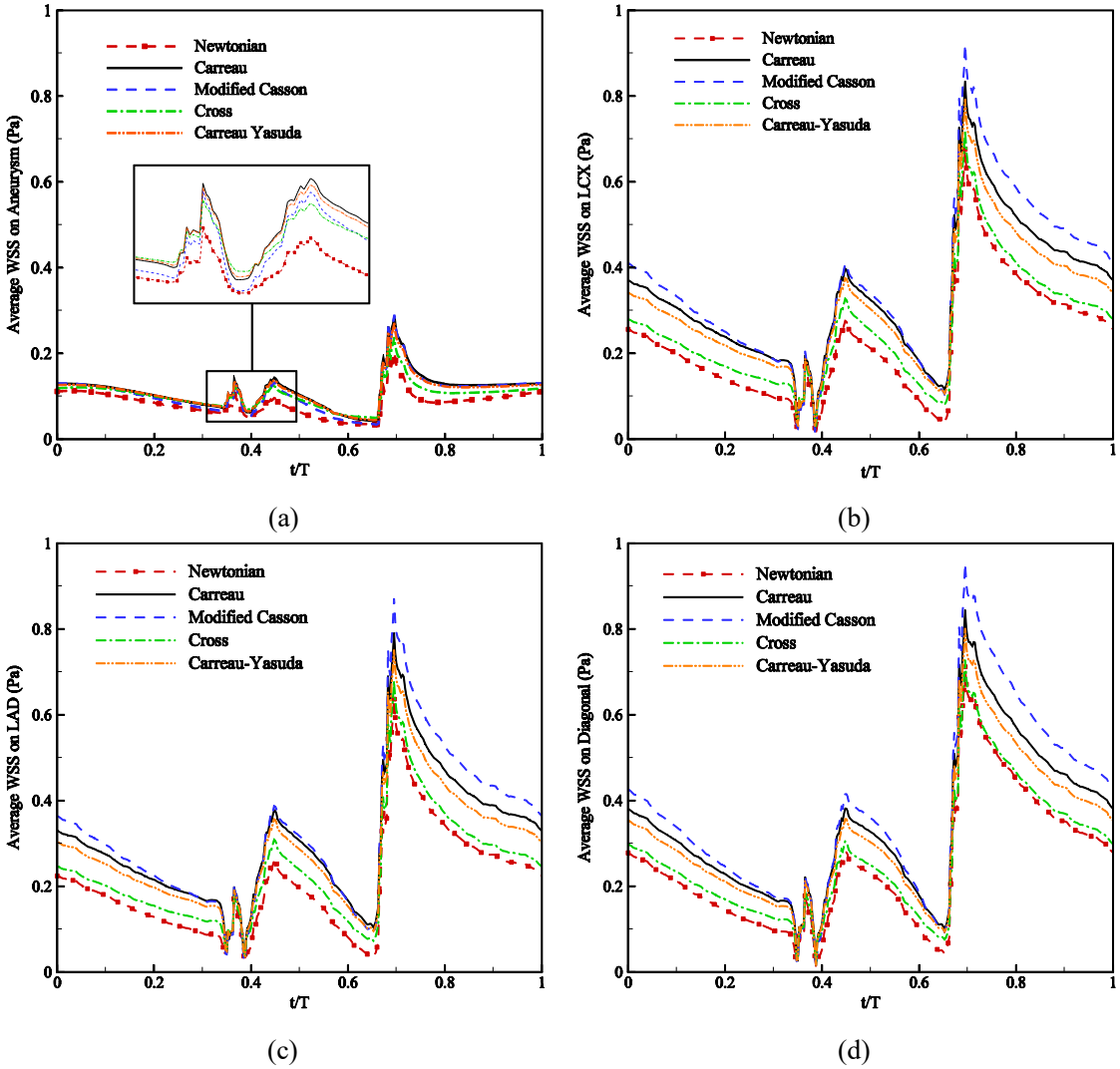

Fig. 13. Average WSS variation in the a) Aneurysm, b) LCX, c) LAD, and d) Diagonal for different viscosity models during the cardiac cycle

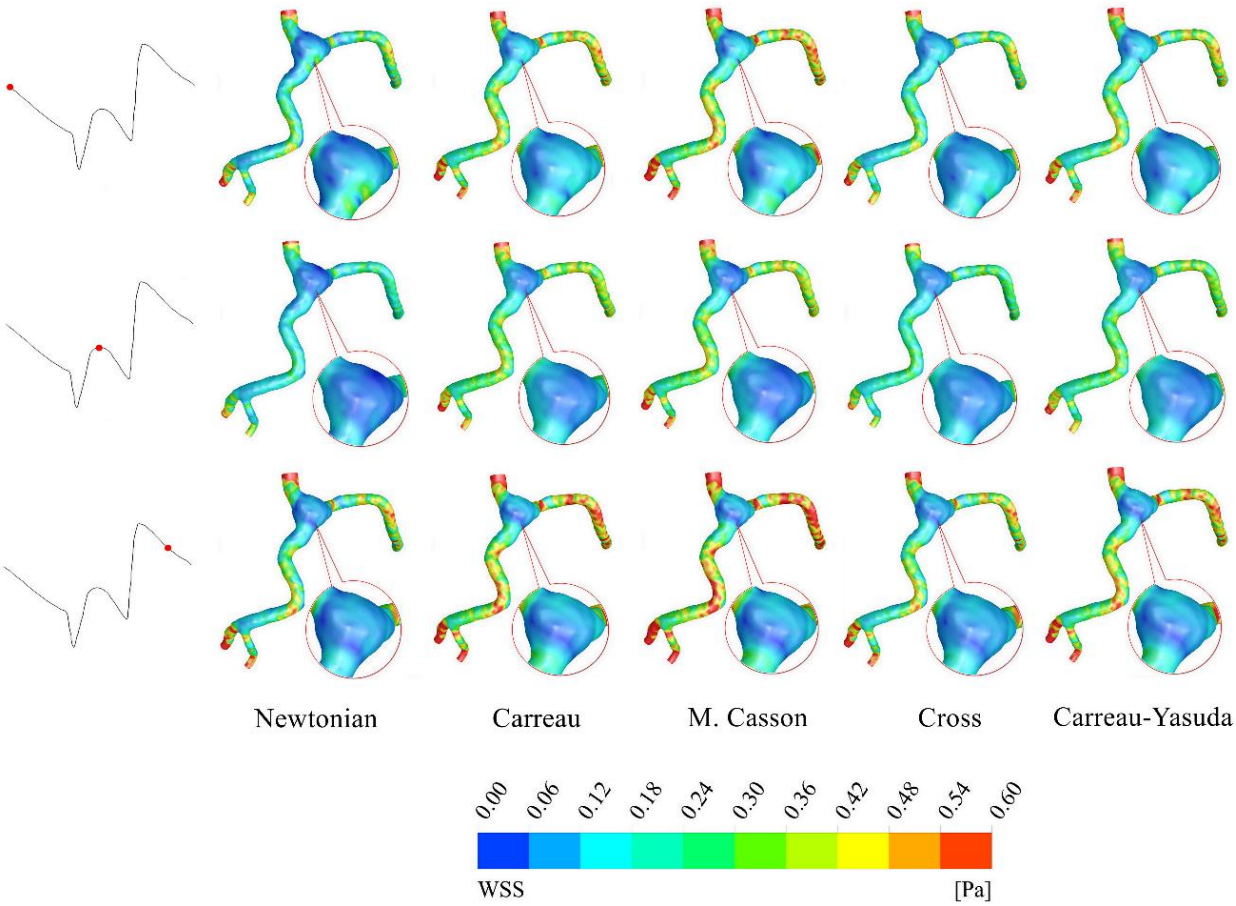

Fig. 14. Contour plots of the WSS distribution in all viscosity models at different pulsatile phases

almost equal for this shear rate range. Moreover, it can be obtained from Table 4 that the most striking discrepancy in the average WSS among non-Newtonian viscosity models is related to the Cross model compared to the Modified Casson model (nearly 28% less than Modified Casson's average WSS). Also, the Cross model predicts the lowest WSS rather than other non-Newtonian viscosity models; because it creates the lowest molecular viscosity at shear rates greater than 10 s^{-1} (close to the Newtonian model). Contrary, the highest value of viscosity has been predicted by the Modified Casson at shear rates above 50 s^{-1}; accordingly, it generates the largest value of average WSS (close to 28% greater than the Cross models, approximately 14% more than Carreau-Yasuda model, and close to 9% greater than Carreau model, in the LCX, LAD, and Diagonal branches over a cardiac cycle). This is despite the fact that the average WSS of the aneurysm during a cardiac cycle calculated by the Carreau model reaches a peak of 0.113 Pa. In other words, up to 8.8% larger than other non-Newtonian models. As stated previously, differences between the results acquired by non-Newtonian models strongly depend on the shear rate scales in the artery; the change of the viscosity as a function of shear rate alters the WSS in various parts of the model.

Fig. 14 shows the WSS distribution contours at t_1, t_2, and t_3. Due to the lower viscosity of the Newtonian model, the area of low WSS estimated by the Newtonian model is larger than the non-Newtonian viscosity models. Also, the Casson model estimates the minimum area of WSS among the non-Newtonian models.

Fig. 15 represents the contours of OSI distribution throughout the LCA for all rheological models. Based on contours for the Carreau, Modified Casson, Cross, and Carreau-Yasuda models, no significant difference is observed between regions with high oscillation shear index, but as shown in Fig 15, the area of regions with high OSI calculated by the Newtonian model is greater than the non-Newtonian viscosity models. It should be noted that in areas with high OSI, the flow and the shear stress vectors, are completely oscillating, and atherosclerotic plaque finds the opportunity to deposit in the endothelial wall of the arteries in these areas. However, it is important to consider that atherosclerosis in the aneurysm -due to its size- does not cause blockage of these parts, but in most cases, it leads to arterial embolism. In other words, the separation of these plaques from the vessel wall and their movement with the bloodstream, as well as the movement of clots formed in aneurysms, causes stenosis

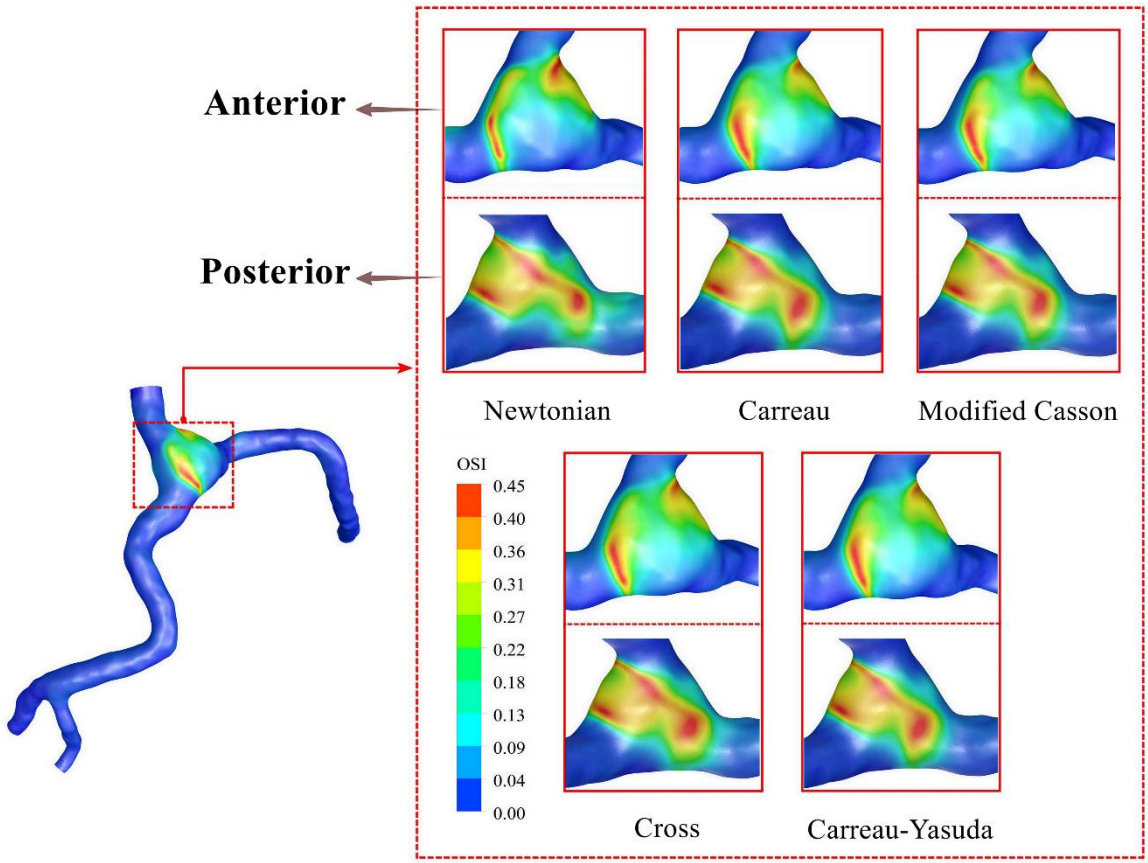

Fig. 15. Oscillatory Shear Index (OSI) in all viscosity models

of small-diameter arteries and thus disrupts blood supply to the heart tissue which in most cases leads to a heart attack or even death.

4- Conclusion

The primary purpose of this study was to provide more details of the effects of blood rheology in the form of increasing and decreasing the blood dynamic viscosity in the Newtonian model on hemodynamic parameters and also compare different non-Newtonian viscosity models. After validation of the simulations and the grid independence test, the effect of the mentioned parameter was studied, and obtained results were presented. Five rheological models, including the Newtonian, Carreau, Modified Casson, Cross, and Carreau-Yasuda models, have been utilized to investigate their effects on the hemodynamic characteristics in the coronary artery aneurysm. The most important results of this analysis are summarized as follows. Due to the direct correlation between blood viscosity and the vessel WSS, the reduction of the blood viscosity declines the vessel WSS, especially in the weakened wall of the aneurysms. On the other hand, an increment of the blood viscosity raises the blood pressure in the coronary artery which increases the WSS of the aneurysm and finally results in a rising aneurysm rupture risk. Therefore, blood-thinning medicines and anticoagulants can dramatically prevent aneurysm rupture and diminish the blood pressure drop in the arteries, which the use of these medicines in incurable aneurysms (i.e., aneurysms located at the bifurcations) is essential as the only way to control the aneurysmal hemodynamic conditions. In the case of comparing Newtonian and non-Newtonian models, blood flow velocity in the Newtonian state is found to be higher than in the non-Newtonian models because of having the lowest blood viscosity and, accordingly, the less frictional resistance in fluid layers. For a similar reason, wall shear stress calculated by the Newtonian model in all segments is less than other rheological models (up to 48%, 59%, 22.6%, and 38% lesser than the Carreau, Modified Casson, Cross, and Carreau-Yasuda models, respectively). The maximum value of the average wall shear stress over a cardiac cycle in different parts of the studied left coronary artery except for the aneurysm (including LAD, LCX, and Diagonal) is related to the Modified Casson models, whereas, in the aneurysm, the Carreau model estimates the average wall shear stress a little more than other rheological models (e.g., around 5.3% larger than Modified Casson). The reason for this is that, at most of the time of the cycle (containing the diastolic phase and top of the systole), the range of the blood strain rate within the LCX, LAD, and Diagonal arteries is above 100 s^{-1} (high strain rate regions), and the Modified Casson has the highest value

of the viscosity in this range. On the other hand, the shear rate of the blood in the aneurysm is less than 40 s^{-1} which means that the viscosity of the Carreau model in this area is slightly more than other applied viscosity models. As is deduced from the results, the Modified Casson overestimates the wall shear stress and non-Newtonian behavior; because mainly generates maximum viscosities in various parts of the LCA, while the Cross model may underrate the blood non-Newtonian behavior due to its similarity to the Newtonian model. Considering hemodynamic conditions not only in the aneurysm but in all sections of the coronary artery, Carreau, and Carreau-Yasuda models demonstrate moderate values of wall shear stress.

Acknowledgments

The authors would like to acknowledge the help of Bistoon Hospital personnel in providing CT-Angiography data.

Conflict of interest

The authors declare that they have no conflict of interest.

References

[1] G.A. Roth, C. Johnson, A. Abajobir, F. Abd-Allah, S.F. Abera, G. Abyu, M. Ahmed, B. Aksut, T. Alam, K. Alam, Global, regional, and national burden of cardiovascular diseases for 10 causes, 1990 to 2015, Journal of the American College of Cardiology, 70(1) (2017) 1-25.

[2] C. Jin, B. Mao, B. Li, Y. Feng, D. Wu, J. Xie, Y. Liu, Hemodynamic Study Of Coronary Artery Aneurysms, Journal of Mechanics in Medicine and Biology, 20(03) (2020) 2050012.

[3] J.B. Gordon, A.M. Kahn, J.C. Burns, When children with Kawasaki disease grow up: Myocardial and vascular complications in adulthood, Journal of the American College of Cardiology, 54(21) (2009) 1911-1920.

[4] Y. Kuramochi, T. Ohkubo, N. Takechi, D. Fukumi, Y. Uchikoba, S. Ogawa, Hemodynamic factors of thrombus formation in coronary aneurysms associated with Kawasaki disease, Pediatrics International, 42(5) (2000) 470-475.

[5] T. Fan, Z. Zhou, W. Fang, W. Wang, L. Xu, Y. Huo, Morphometry and hemodynamics of coronary artery aneurysms caused by atherosclerosis, Atherosclerosis, 284 (2019) 187-193.

[6] M. Abbasian, M. Shams, Z. Valizadeh, A. Moshfegh, A. Javadzadegan, S. Cheng, Effects of different non-Newtonian models on unsteady blood flow hemodynamics in patient-specific arterial models with in-vivo validation, Computer methods and programs in biomedicine, 186 (2020) 105185.

[7] K. Haldar, Effects of the shape of stenosis on the resistance to blood flow through an artery, Bulletin of Mathematical Biology, 47(4) (1985) 545-550.

[8] S.P. Shupti, M.G. Rabby, M. Molla, Rheological behavior of physiological pulsatile flow through a model arterial stenosis with moving wall, Journal of Fluids, Article ID546716, (2015).

[9] B.M. Johnston, P.R. Johnston, S. Corney, D. Kilpatrick, Non-Newtonian blood flow in human right coronary arteries: steady state simulations, Journal of biomechanics, 37(5) (2004) 709-720.

[10] G. Lorenzini, Blood velocity field numerical assessment using a GPL code in case of intravascular Doppler catheter affections: comparative analysis of different rheological models, Journal of biomechanics, 38(10) (2005) 2058-2069.

[11] Y. Fan, W. Jiang, Y. Zou, J. Li, J. Chen, X. Deng, Numerical simulation of pulsatile non-Newtonian flow in the carotid artery bifurcation, Acta Mechanica Sinica, 25(2) (2009) 249-255.

[12] X. Wang, X. Li, Computational simulation of aortic aneurysm using FSI method: influence of blood viscosity on aneurismal dynamic behaviors, Computers in biology and medicine, 41(9) (2011) 812-821.

[13] A. Skiadopoulos, P. Neofytou, C. Housiadas, Comparison of blood rheological models in patient specific cardiovascular system simulations, Journal of Hydrodynamics, Ser. B, 29(2) (2017) 293-304.

[14] A. Caballero, S. Laín, Numerical simulation of non-Newtonian blood flow dynamics in human thoracic aorta, Computer methods in biomechanics and biomedical engineering, 18(11) (2015) 1200-1216.

[15] A.J. Apostolidis, A.P. Moyer, A.N. Beris, Non-Newtonian effects in simulations of coronary arterial blood flow, Journal of Non-Newtonian Fluid Mechanics, 233 (2016) 155-165.

[16] C. Oliveira, A.A. Soares, A. Simões, S. Gonzaga, A. Rouboa, Numerical study of non-Newtonian blood behavior in the abdominal aortic bifurcation of a patient-specific at rest, The Open Sports Sciences Journal, 10(1) (2017).

[17] S.E. Razavi, V. Farhangmehr, N. Zendeali, Numerical investigation of the blood flow through the middle cerebral artery, Bioimpacts, 8(3) (2018) 195-200.

[18] S. Bahrami, M. Norouzi, A numerical study on hemodynamics in the left coronary bifurcation with normal and hypertension conditions, Biomechanics and modeling in mechanobiology, 17(6) (2018) 1785-1796.

[19] M. Kopernik, P. Tokarczyk, Development of multi-phase models of blood flow for medium-sized vessels with stenosis, Acta of bioengineering and biomechanics, 21(2) (2019).

[20] A. Razavi, E. Shirani, M.R. Sadeghi, Numerical simulation of blood pulsatile flow in a stenosed carotid artery using different rheological models, Journal of biomechanics, 44(11) (2011) 2021-2030.

[21] T. Chaichana, Z. Sun, J. Jewkes, Computation of hemodynamics in the left coronary artery with variable angulations, Journal of biomechanics, 44(10) (2011) 1869-1878.

[22] S.E. Razavi, V. Farhangmehr, Z. Babaie, Numerical investigation of hemodynamic performance of a stent in the main branch of a coronary artery bifurcation, Bioimpacts, 9(2) 97-103.

[23] D. Sengupta, A.M. Kahn, J.C. Burns, S. Sankaran, S.C. Shadden, A.L. Marsden, Image-based modeling of hemodynamics in coronary artery aneurysms caused

by Kawasaki disease, Biomechanics and modeling in mechanobiology, 11(6) (2012) 915-932.

[24] I. ANSYS, (2016), ANSYS Fluent User's Guide, Release 17.1.

[25] Y.I. Cho, K.R. Kensey, Effects of the non-Newtonian viscosity of blood on flows in a diseased arterial vessel. Part 1: Steady flows, Biorheology, 28(3-4) (1991) 241-262.

[26] H.A. González, N.O. Moraga, On predicting unsteady non-Newtonian blood flow, Applied Mathematics and Computation, 170(2) (2005) 909-923.

[27] S. Karimi, M. Dabagh, P. Vasava, M. Dadvar, B. Dabir, P. Jalali, Effect of rheological models on the hemodynamics within human aorta: CFD study on CT image-based geometry, Journal of Non-Newtonian Fluid Mechanics, 207 (2014) 42-52.

[28] A. Buradi, A. Mahalingam, Numerical Analysis of Wall Shear Stress Parameters of Newtonian Pulsatile Blood Flow Through Coronary Artery and Correlation to Atherosclerosis, in: B.B. Biswal, B.K. Sarkar, P. Mahanta (Eds.) Advances in Mechanical Engineering, Springer Singapore, Singapore, 2020, pp. 107-118.

[29] D.N. Ku, D.P. Giddens, C.K. Zarins, S. Glagov, Pulsatile flow and atherosclerosis in the human carotid bifurcation. Positive correlation between plaque location and low oscillating shear stress, Arteriosclerosis (Dallas, Tex.), 5(3) (1985) 293-302.

[30] X. He, D.N. Ku, Pulsatile flow in the human left coronary artery bifurcation: average conditions, Journal of biomechanical engineering, 118(1) (1996) 74-82.

[31] C. Chiastra, S. Morlacchi, D. Gallo, U. Morbiducci, R. Cárdenes, I. Larrabide, F. Migliavacca, Computational fluid dynamic simulations of image-based stented coronary bifurcation models, Journal of The Royal Society Interface, 10(84) (2013) 20130193.

[32] K.E. Barrett, S. Boitano, S.M. Barman, H.L. Brooks, Ganong's review of medical physiology twenty, (2010).

[33] E. Boutsianis, H. Dave, T. Frauenfelder, D. Poulikakos, S. Wildermuth, M. Turina, Y. Ventikos, G. Zund, Computational simulation of intracoronary flow based on real coronary geometry, European journal of Cardio-thoracic Surgery, 26(2) (2004) 248-256.

[34] D. Sengupta, A.M. Kahn, E. Kung, M.E. Moghadam, O. Shirinsky, G.A. Lyskina, J.C. Burns, A.L. Marsden, Thrombotic risk stratification using computational modeling in patients with coronary artery aneurysms following Kawasaki disease, Biomechanics and modeling in mechanobiology, 13(6) (2014) 1261-1276.

[35] F.J.H. Gijsen, F.N. van de Vosse, J.D. Janssen, The influence of the non-Newtonian properties of blood on the flow in large arteries: steady flow in a carotid bifurcation model, Journal of biomechanics, 32(6) (1999) 601-608.

[36] I. Chatziprodromou, A. Tricoli, D. Poulikakos, Y. Ventikos, Haemodynamics and wall remodelling of a growing cerebral aneurysm: a computational model, Journal of biomechanics, 40(2) (2007) 412-426

HOW TO CITE THIS ARTICLE

A. Rafiei, M. Saidi, Numerical Evaluation on Blood Rheological Behavior in a Realistic Model of Aneurysmal Coronary Artery , AUT J. Mech Eng., 6(4) (2022) 579-596.

DOI: 10.22060/ajme.2022.20917.6025